Multiple magnetic ordering phenomena evaluated by heat capacity measurements in $Er_{1-x}Tb_xAl_2$ Laves-phase alloys

Mahmud Khan
The Ames Laboratory, U.S. Department of Energy, Iowa State University, Ames, Iowa 50011-3020, USA

K. A. Gschneidner, Jr. and V. K. Pecharsky
The Ames Laboratory, U.S. Department of Energy, Iowa State University, Ames, Iowa 50011-3020, USA
and Department of Materials Science and Engineering, Iowa State University, Ames, Iowa 50011-2300, USA
(Received 7 October 2009; revised manuscript received 6 November 2009; published 7 December 2009)

Heat capacity measurements in zero and applied magnetic fields have been performed on a series of $Er_{1-x}Tb_xAl_2$ pseudobinary Laves-phase alloys. Different anomalies that change with Tb concentrations have been observed. These anomalies represent multiple magnetic ordering phenomena, similar to those reported in $Er_{1-x}Pr_x$ and $Er_{1-x}Dy_xAl_2$ alloys. In common, all alloys contain mixtures of lanthanide metals with opposite signs of the second-order Steven's operators, which were believed to cause competition between the magnetoelastic, crystalline electric field, and quadrupolar effects. This competition gives rise to the observed multiple magnetic ordering transitions in $Er_{1-x}Pr_x$ and $Er_{1-x}Dy_xAl_2$ alloys. Tb and Er also have opposite signs of second-order Steven's factors, and therefore the observed anomalies in the $Er_{1-x}Tb_xAl_2$ alloys may also be interpreted in terms of competing quadrupolar, magnetoelastic, and crystalline electric field effects. The magnetocaloric properties of the $Er_{1-x}Tb_xAl_2$ alloy system have also been evaluated.

DOI: 10.1103/PhysRevB.80.224408 PACS number(s): 75.10.Dg, 71.20.Lp, 74.25.Ha, 75.30.Sg

I. INTRODUCTION

For almost half a century the magnetic and physical properties of RAl_2 (R=rare earth metal) compounds have been thoroughly studied by both experimental and theoretical approaches.[1–7] These and other investigations have revealed many interesting properties of the RAl_2 family, both from fundamental scientific and applied points of view. The RAl_2 compounds adopt the cubic Laves-phase $MgCu_2$-type structure, and they order ferromagnetically at various Curie temperatures which are dependent on the nature of the R atom.[6,7] Although their basic magnetic properties such as, ferromagnetic ordering temperatures, crystal structures, magnetic anisotropy, etc., are known for a long time, some significant and interesting properties of the RAl_2 alloys were not discovered until recently.

Initially for fundamental investigation by Swift and Wallace,[8] and later in an effort to develop active magnetic regenerator (AMR) materials for hydrogen liquefaction, Er in $ErAl_2$ was partially replaced by Dy.[9] It was shown that $Dy_{0.5}Er_{0.5}Al_2$ is an excellent alternative to GdPd as an AMR material.[10] While conducting this experimental study, a sequence of disappearing and appearing magnetic phases was discovered as Er was replaced with Dy in the $Er_{1-x}Dy_xAl_2$ system.[9,11] Over a wide range of Dy concentrations centered around x=0.25, first-order phase transitions were observed in the heat capacity data of the respective members of this alloy system. The transition then disappeared with further Dy addition. These additional transitions were observed below T_C of the respective alloys. In the vicinity of the first-order transition, unusual anomalies were observed in magnetization and ac magnetic susceptibility as well.[12]

A similar behavior has also been reported to exist in $Er_{1-x}Pr_x$ compounds.[13–15] Most interestingly, both the $Er_{1-x}Dy_xAl_2$ and $Er_{1-x}Pr_x$ alloy systems share a common property. Each system contains a combination of rare-earth elements whose second-order Steven's operators are of opposite signs.[16] In other words, the 4f-electron charge densities of the Dy^{3+} and Pr^{3+} are oblate spheroids, whereas for the Er^{3+} the 4f-electron charge density is a prolate spheroid. These three elements are known to exhibit crystalline electric field effects and possible magnetoelastic and quadrupolar effects. Therefore, in a compound containing a mixture of two such elements with different 4f charge distribution, the indirect (Ruderman-Kittel-Kasuya-Yoshida) exchange interactions, crystal field, and the quadrupolar interactions may be modified, altering the magnetic properties of the compound. Lima *et al.*[11] showed that the appearance and disappearance of the first-order phase transition in $Er_{1-x}Dy_xAl_2$ is a result of competing magnetoelastic coupling and quadrupolar effects.

Considering the RAl_2 compounds, it is interesting to explore if such behavior is limited only to the $Er_{1-x}Dy_xAl_2$ and $Er_{1-x}Pr_x$ systems or not. If combining rare-earth elements with opposite signs of second-order Steven's factors can give rise to such effects, then similar behaviors should also be observed when other rare-earth elements such as Tb is used instead of Dy or Pr to replace Er. In this paper we present an experimental study of a series of $Er_{1-x}Tb_xAl_2$ alloys in order to explore the effects of Tb doping in $Er_{1-x}Tb_xAl_2$.

II. EXPERIMENTAL DETAILS

The Tb and Er metals used to prepare the $Er_{1-x}Tb_xAl_2$ ($0 \le x \le 1$) alloys were obtained from the Materials Preparation Center of the Ames Laboratory[17] and were 99.8+at. % pure with the following major impurities (in ppm atomic): Er—O(42), C(320), N(36), F(62), Fe(263) and Tb—O(199), C(105), N(12), F(37), H(135), Fe(4.9). The Al metal of 5N purity was purchased from Alfa Aesar Inc. Polycrystalline buttons of $Er_{1-x}Tb_xAl_2$ (x=0, 0.1, 0.15, 0.20, 0.25, 0.30,

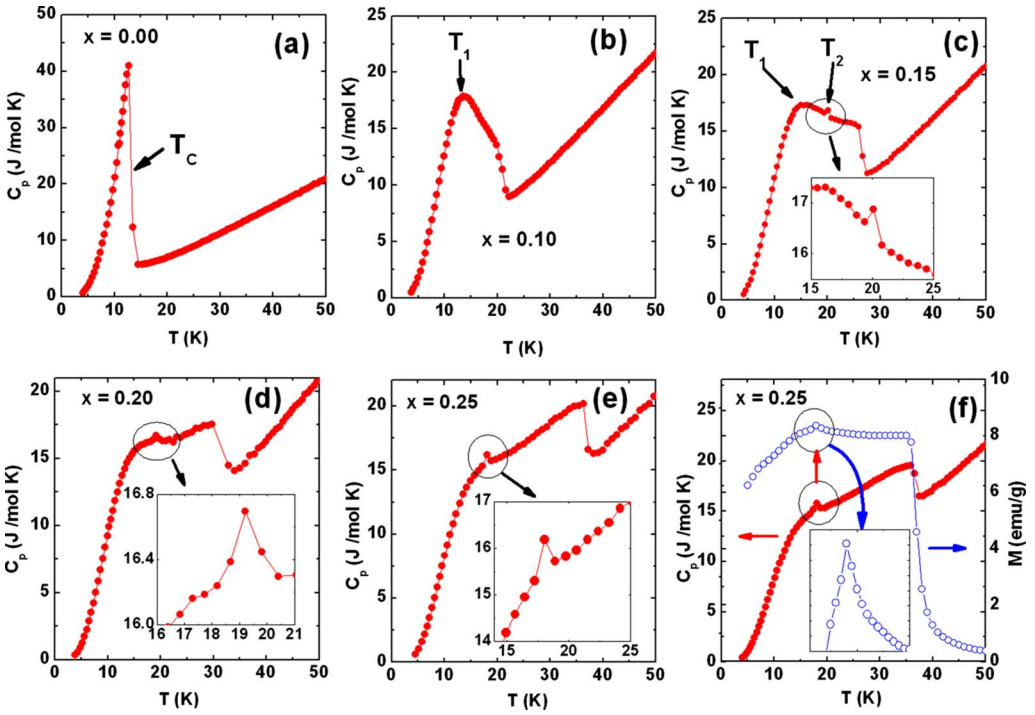

FIG. 1. (Color online). Heat capacity (C_P) data of $Er_{1-x}Tb_xAl_2$ ($0 \leq x \leq 0.25$) measured as a function of temperature in zero magnetic field. The zero magnetic field C_P data and the corresponding ZFC magnetization versus temperature data measured in a magnetic field of 100 Oe of $Er_{1-x}Tb_xAl_2$ for $x=0.25$ are shown in panel (f).

0.35, 0.50, 0.75, and 0.90) alloys weighing approximately 5 g each were prepared by conventional arc melting technique in an argon atmosphere. The alloys melt congruently, and therefore, annealing was not necessary. The phase purities of the samples were checked by x-ray powder diffraction measurements and all of them were found to be single phase. A home made adiabatic heat-pulse calorimeter was used to conduct the heat capacity measurements.[18] The measurements were performed in the temperature range from ~3.8 to 300 K in zero magnetic field and in applied magnetic fields up to 5 T. The dc magnetization was measured using a superconducting quantum interference device magnetometer MPMS XL-7 made by Quantum Design Inc.

III. EXPERIMENTAL RESULTS AND DISCUSSION

Figure 1 shows the heat capacities of $Er_{1-x}Tb_xAl_2$ with $0.0 \leq x \leq 0.25$ measured as a function of temperature. With increasing temperature, heat capacity of the alloy with $x=0$ (pure $ErAl_2$) increases sharply until it reaches a peak at 12.7 K [Fig. 1(a)]. This λ-type peak, which indicates a second-order magnetic disordering transition, is followed by a sharp drop of the heat capacity at the Curie temperature, T_C. This is the only transition observed in the heat capacity of $ErAl_2$, and the observation is consistent with previously reported results.[9,11]

Even a small addition of Tb ($x=0.1$) transforms the heat capacity [Fig. 1(b)] so that the sharp λ-type peak becomes much broader. After reaching a broad maximum (we refer to this peak as peak B and the corresponding temperature as T_1) around 13.5 K, the heat capacity decreases gradually and with further increase in temperature it sharply drops at T_C. Immediately above T_C, the heat capacity increases almost linearly with temperature up to 50 K. As the Tb concentration is increased, a third peak in the heat capacity of $Er_{1-x}Tb_xAl_2$ develops between a broad peak B and T_C. We refer to this peak as peak C and the corresponding temperature as T_2 [see Fig. 1(c) through Fig. 1(e)]. As shown in the insets of Figs. 1(c) and 1(d), the weak but sharp anomalies represented by peak C indicate first-order phase transitions. Since all of the peaks C are represented by a single datum, indicating that transitions at T_2 are narrow, reproducibility of the results has been verified by repeating the measurements in the vicinity of T_2. The sharp anomalies (peak C at T_2) are observed in each measurement. The errors in heat capacity are below 0.7%,[18] and the error bars are smaller than the size of the symbols on the plots.

The anomaly at T_2 has been verified by measurements of the low field magnetization. Figure 1(f) shows the zero-field-cooled (ZFC) magnetization versus temperature data measured in a magnetic field of 100 Oe, and the zero magnetic field heat capacity of $Er_{1-x}Tb_xAl_2$ for $x=0.25$. The inset shows the nature of the transition in magnetization around T_2. As shown in Fig. 1(f), the sharp anomaly observed in the zero-field heat capacity agrees well with the low field magnetization versus temperature data.

The heat capacities of the $Er_{1-x}Tb_xAl_2$ alloys with $0.30 \leq x \leq 0.90$ are shown in Fig. 2. As the fraction of substituting Tb atoms exceeds 0.25, the sharp peak C disappears. Beyond this concentration ($x > 0.25$), peak B becomes more and more broadened with increasing Tb concentration and it finally disappears for $x > 0.75$. In the alloys with $x > 0.75$, the only transitions that are clearly observed are the

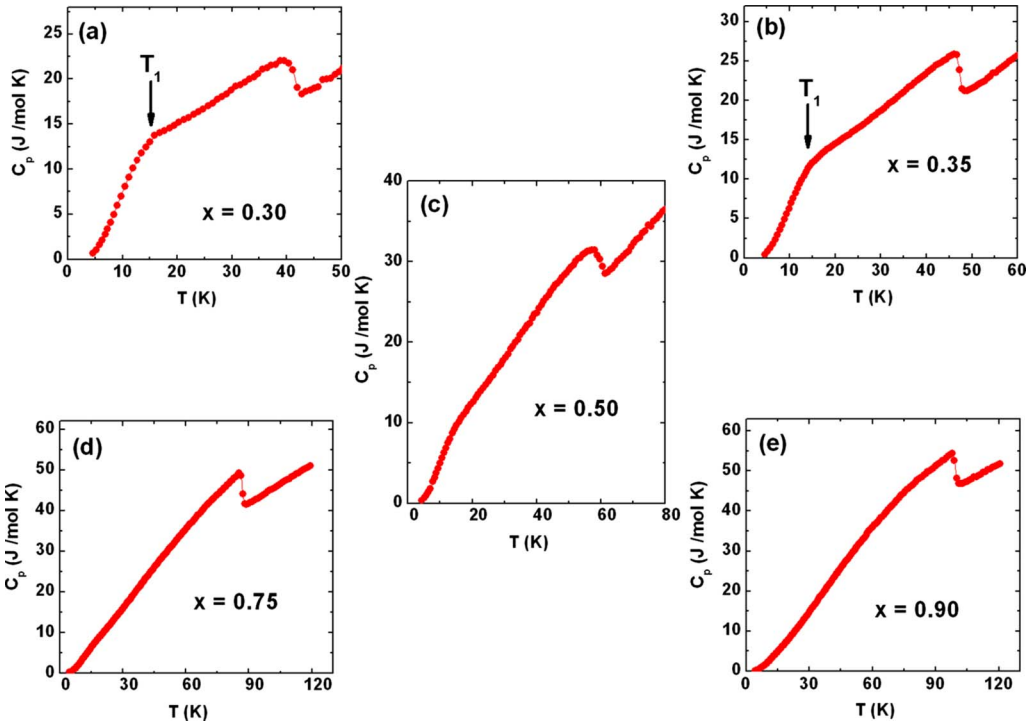

FIG. 2. (Color online). Heat capacity (C_P) data of $Er_{1-x}Tb_xAl_2$ ($0.35 \leq x \leq 0.90$) measured as a function of temperature in zero magnetic field.

paramagnetic/ferromagnetic transitions at T_C.

Figure 3 represents a plot of T_C, T_1, and T_2 as a function of Tb concentration x of $Er_{1-x}Tb_xAl_2$. It can clearly be seen that the T_C of the system increases nearly linearly with increasing Tb concentration. This behavior is expected due to the fact that the De Gennes factor of Tb (0.667) is higher than that of Er (0.162). It is interesting to note that the temperature, T_1, of peak B remains nearly constant with increasing Tb concentration x, while the temperature, T_2, of peak C decreases linearly. When x exceeds 0.25, T_2 merges with T_1. When $x \leq 0.1$, T_2 merges with T_C. In either case, peak C is no longer observed. In case of $Er_{1-x}Dy_xAl_2$, peaks identical to B and C are also present with the exception that the magnitude of peak C is much greater in the Dy alloys.[11] With increasing Dy concentration, the temperature of peak B (T_1) in $Er_{1-x}Dy_xAl_2$ also remains unchanged while peak C (at T_2) shifts toward lower temperature, and once peak T_2 merges with T_1 only a broad peak B remains discernible. For $x < 0.14$ peak C at T_2 also disappears in $Er_{1-x}Dy_xAl_2$ as T_2 merges with T_C. Basically the two systems behave in a similar way.

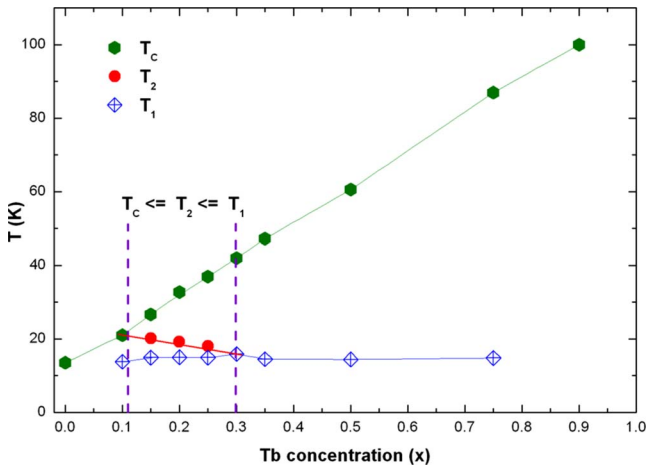

FIG. 3. (Color online). Ferromagnetic transition temperatures, T_C, and temperatures of peaks, B (T_1) and C (T_2), as a function of the Tb concentration (x) of $Er_{1-x}Tb_xAl_2$.

As mentioned earlier, the emergence of peaks B and C in $Er_{1-x}Dy_xAl_2$ was related to a competition between quadrupolar and magnetoelastic effects.[11] When the magnetoelastic coupling dominates, peak C was apparent, and when the quadrupolar terms dominate, the broader peak B was seen. Both the quadrupolar terms and magnetoelastic coupling are dependent on the second-order Steven's factors of the R^{3+} ions, and the competition was mainly attributed to the signs of the Steven's factors of Er^{3+} and Dy^3 being opposite. The second-order Steven's factor of Tb^{3+} has the same sign as that of Dy^{3+}. However, the magnitude of the factor for Tb^{3+} is much smaller $(-1/99)$ compared to $(-2/9.35)$ for Dy^{3+}, which means that the $4f$ charge density of the Tb^{3+} ion is much closer to a sphere. Therefore, the magnetoelastic coupling and quadrupolar terms in $Er_{1-x}Dy_xAl_2$ and $Er_{1-x}Tb_xAl_2$ are expected to be different.

The quadrupolar interactions usually consist of two contributions one of which is associated with the biquadratic coupling of spins that leads to quadrupolar exchange via indirect Coulomb and exchange interactions. The second contribution originates from the coupling of the lattice with the $4f$ shell quadrupoles that result in magnetoelastic effects. In fact magnetoelastic effects caused by lattice quadrupole in-

teractions have been observed in quite a few systems.[19–22] Therefore it is also lucid to suggest that the magnetoelastic coupling responsible for the emergence of peak C is an outcome of the lattice quadrupole coupling. In other words when the coupling of the lattice with the $4f$ shell quadrupole prevails, peak C becomes apparent, while peak B is apparent when the other quadrupole components are strong. Although low-temperature x-ray diffraction measurements showed that in the $Er_{1-x}Dy_xAl_2$ system no structural transition takes place in the vicinity of peak C, unit-cell-volume anomaly was observed in the vicinity of the peak.[12] This behavior suggests that some magnetoelastic effects do exist in the vicinity of peak C in $Er_{1-x}Dy_xAl_2$.

Since the number of $4f$ electrons of Dy and the magnitude of its second-order Steven's factor are both greater than those of Tb, the lattice quadrupole coupling in $Er_{1-x}Dy_xAl_2$ is stronger than it is in $Er_{1-x}Tb_xAl_2$. Due to this stronger lattice quadrupole coupling the peak C is strong and sharp in $Er_{1-x}Dy_xAl_2$, and it is the only peak observed once it merges with peak B. Whereas, due to the weaker lattice quadrupole coupling in $Er_{1-x}Tb_xAl_2$ system the peak C is weak and it disappears once it merges with peak B. The easy suppression of peak C upon the application of a magnetic filed also supports this explanation. The applied magnetic field enhances the magnetic exchange interaction energy, and thus, diminishes the quadrupolar effects.

The spin-reorientation effects in $Er_{1-x}Dy_xAl_2$ and $Er_{1-x}Tb_xAl_2$ are also expected to be different. This is because, the easy magnetization axes of $ErAl_2$ and $DyAl_2$ are different, [111] $ErAl_2$ and [100] $DyAl_2$, whereas they are the same for $ErAl_2$ and $TbAl_2$.[6] Also, $DyAl_2$ is known to exhibit a spin-reorientation transitions,[9] whereas no such transitions have been reported for either $ErAl_2$ or $TbAl_2$. As a result, one may expect that the $Er_{1-x}Dy_xAl_2$ system should exhibit spin reorientation at some low concentrations of Er, which, in fact, have been reported to occur.[9] On the other hand, since neither $ErAl_2$ nor $TbAl_2$ exhibit spin-reorientation transitions one may expect the absence of such transitions in $Er_{1-x}Tb_xAl_2$ systems as well.

In order to estimate the magnetic entropy involved in multiple magnetic ordering transformations occurring in $Er_{1-x}Tb_xAl_2$ system, the magnetic contributions to the heat capacities (C_M) were evaluated by subtracting the prorated heat capacities of nonmagnetic $LaAl_2$ and $LuAl_2$ from the heat capacities of $Er_{1-x}Tb_xAl_2$ samples. This was done under the assumption that the lattice and electronic contributions to the heat capacity vary linearly with atomic number across the lanthanide series. After the subtraction, the magnetic entropy was computed as $S_M = \int_{T_0}^{T} \frac{C_M}{T} dT$, where T_0 is the lowest temperature of the measurements.

The magnetic entropies as a function of temperature in zero magnetic field are shown in Fig. 4. In pure $ErAl_2$, S_M increases sharply with increasing temperature until T_C, where a change in slope is observed that leads to the saturation of the magnetic entropy. The S_M at T_C is 14.9 J/mol K, which is 64% of the theoretical limit, $S_M^{\text{Theory}} = R \ln(2J+1) = 23.1$ J/mol K. At 40 K above T_C, the value of S_M in $ErAl_2$ reaches 21.3 J/mol K, which is about 92% of the theoretical limit. These results are consistent with the previously reported results.[9] As the concentration of Tb in the $Er_{1-x}Tb_xAl_2$ system increases, the S_M released at T_C also increases, whereas the total S_M decreases, as expected from the difference of the total angular momentum of Er (15/2) and Tb (12/2). This is illustrated in Fig. 5, where the magnetic entropies at T_C, the total magnetic entropies, and the theoretical magnetic entropies are plotted as a function of the Tb concentration x. For the $Er_{1-x}Tb_xAl_2$ alloy system the theoretical limit decreases from 23.1 J/mol K (for $x=0$) to 21.5 J/mol K (for $x=0.9$). The experimental S_M values 40 K above the respective T_C of each of the alloy in the system are between 89 to 94% of the theoretical entropy.

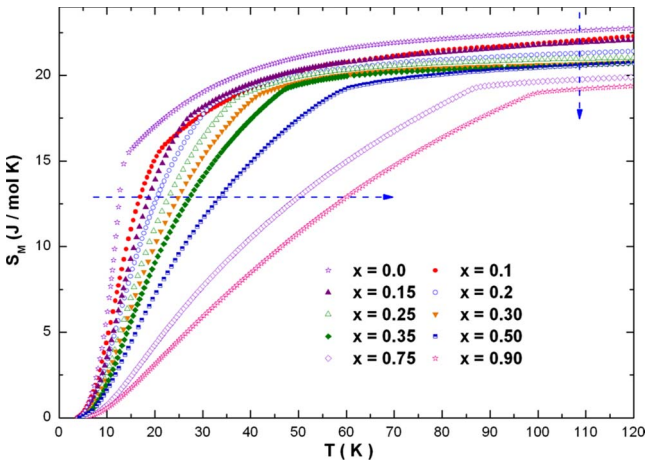

FIG. 4. (Color online). Magnetic entropies in a zero magnetic field of $Er_{1-x}Tb_xAl_2$ as a function of temperature. The arrows in the figure indicate the increase in the Tb concentration (x).

Another common feature present in both $Er_{1-x}Dy_xAl_2$ and $Er_{1-x}Pr_x$ systems is the disappearance of the sharp peak of the heat capacity with the application of an external magnetic field.[9,14] In order to verify if a similar behavior exists in $Er_{1-x}Tb_xAl_2$, we carried out heat capacity measurements in applied magnetic fields for selected samples from the $Er_{1-x}Tb_xAl_2$ series. Figure 6 illustrates the heat capacity of

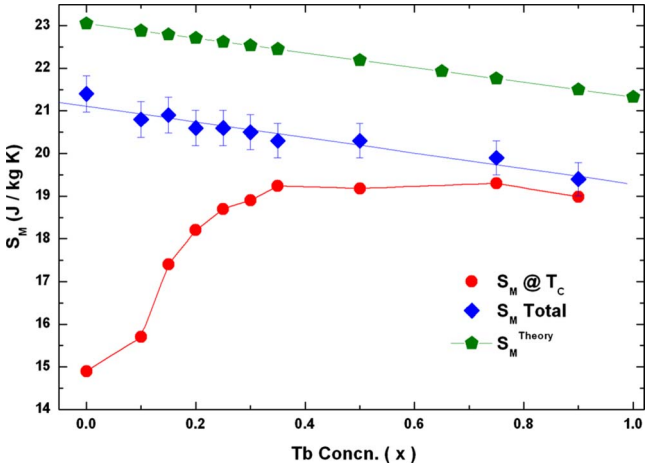

FIG. 5. (Color online). Magnetic entropies at T_C (S_M @ T_C), magnetic entropies at 40 K above T_C (S_M total), and theoretical magnetic entropies (S_M^{Theory}) of $Er_{1-x}Tb_xAl_2$ as functions of temperature in a zero magnetic field.

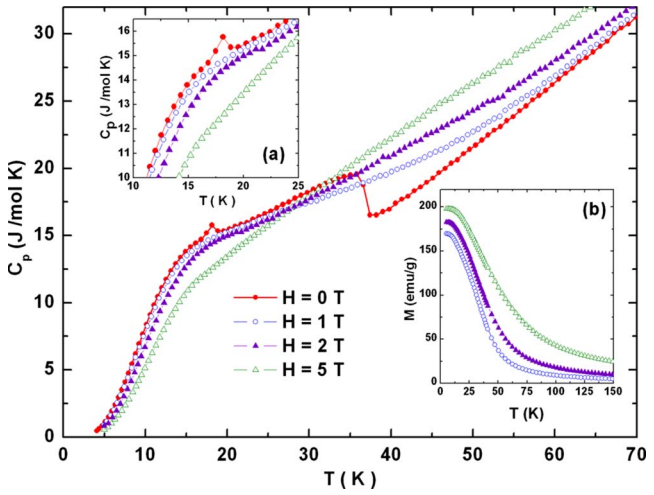

FIG. 6. (Color online). Heat capacity of $Er_{1-x}Tb_xAl_2$ (x=0.25) as a function of temperature measured in different magnetic fields. Inset (a) clarifies behavior around T_2. Inset (b) shows the magnetization versus temperature measured in same magnetic fields.

$Er_{1-x}Tb_xAl_2$ (x=0.25) as a function of temperature measured in applied magnetic fields ranging from 0 to 5 T. The sharp peak in the heat capacity is no longer observed when a magnetic field of 1 T is applied. The sharp transition at T_C is also found to disappear as external magnetic fields are applied. Figure 6 also shows that below T_C the magnetic heat capacity is lowered, and above T_C the magnetic heat capacity becomes greater than the zero-field heat capacity. This behavior is typical for a ferromagnetic material. The inset (b) of Fig. 6 shows that the application of magnetic field causes the disappearance of the sharp peak that is seen in the low field magnetization versus temperature data [see Fig. 1(f)]. This behavior is in agreement with the behavior of the heat capacity measured in same magnetic fields.

The magnetic entropy changes, ΔS_M, were evaluated by subtracting the total entropy curves obtained in an applied magnetic field from the zero-field total entropy curves of $Er_{1-x}Tb_xAl_2$. Figure 7 shows the magnetic entropy changes, ΔS_M, as a function of temperature of $Er_{1-x}Tb_xAl_2$ for x=0.25 and 0.35. As shown in Fig. 7(a), the ΔS_M curves of the alloys for a 1 T field change show two peaks. The first peak is observed around 19 K for both alloys, whereas the second peak is observed around 36.6 and 47 K, for the alloys with x=0.25 and 0.35, respectively. The peak at 19 K reflects the same anomalies that lead to the appearance of peaks B and C in the heat capacity data. The peaks at 36.6 and 47 K represent the T_C's of respective alloys.

Although the nature of ΔS_M curves of the two alloys for a 1 T field change is quite similar, as the magnitude of the applied magnetic field increases the behavior of the two curves becomes different [see Figs. 7(a) and 7(b)]. For a 2 T field change, the peak at 19 K nearly disappears in the alloy with x=0.25, but it still remains in the alloy with x=0.35. For a 5 T field change, the 19 K peak is no longer visible in either of the alloys. These differences in the ΔS_M curves of the alloys with x=0.25 and 0.35 are most probably again due to the differences in the lattice quadrupole coupling in the two alloys.

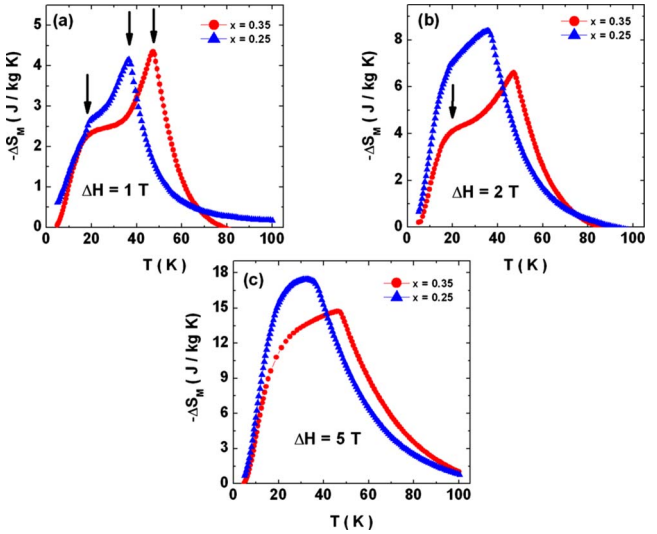

FIG. 7. (Color online). Magnetic entropy change, ΔS_M, in $Er_{1-x}Tb_xAl_2$ (x=0.25 and 0.35) as a function of temperature for three different magnetic field changes.

Figure 8 shows the adiabatic temperature changes, ΔT_{ad}, of $Er_{1-x}Tb_xAl_2$ for x=0.25 and 0.35 as a function of temperature calculated from the heat capacity data. The peaks of the ΔT_{ad} vs T plots are the respective Curie temperatures of the alloys. Both the ΔS_M and ΔT_{ad} curves show asymmetric behavior, which was also seen in $Er_{1-x}Dy_xAl_2$ for certain values of x.[9,11] For a 5 T field change the refrigeration capacities (i.e., relative cooling power)[23] are found to be 570(40) J/kg and 650(45) J/kg (see Ref. 24 for details on calculating the uncertainties) for the alloys with x=0.25 and 0.35, respectively. These values, together with the reasonably high ΔT_{ad} values, make the $Er_{1-x}Tb_xAl_2$ alloys promising as AMR materials for hydrogen liquefaction.

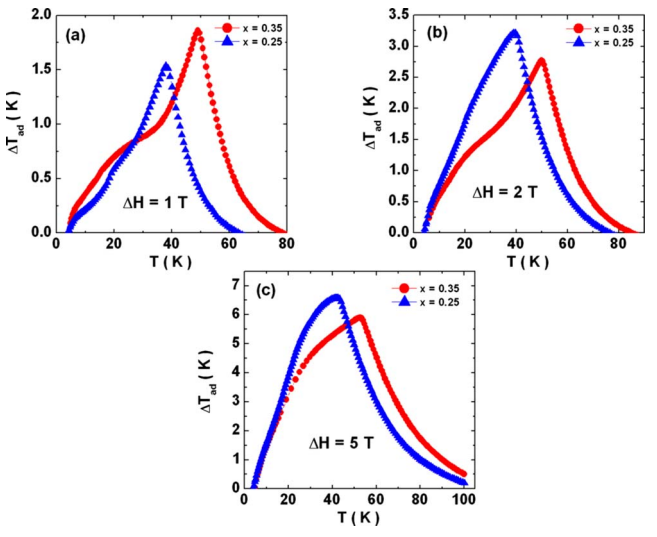

FIG. 8. (Color online). Adiabatic temperature change, ΔT_{ad}, in $Er_{1-x}Tb_xAl_2$ (x=0.25 and 0.35) as a function of temperature for three different magnetic field changes.

IV. CONCLUSIONS

The addition of Tb increases the ferromagnetic transition temperature T_C and decreases the total magnetic entropies of $Er_{1-x}Tb_xAl_2$ alloys in zero magnetic fields. The experimental observations revealed the existence of multiple magnetic transitions in the alloys. For certain Tb concentration ($0.15 \leq x \leq 0.25$), weak but sharp anomalies have been observed in the heat capacity curves, which disappear with increasing Tb concentration and are easily suppressed by the magnetic field (≤ 1 T). The sharp anomalies are believed to appear because of magnetoelastic effects caused by the coupling of the lattice with the $4f$ shell quadrupoles. The magnitudes of the sharp anomalies are not as great as they are in previously reported $Er_{1-x}Dy_xAl_2$ alloys. These differences are attributed to the differences in the number of $4f$ electrons and the magnitude of the second-order Steven's factors of Dy and Tb. In addition to multiple magnetic transitions, the $Er_{1-x}Tb_xAl_2$ alloys exhibit substantial magnetocaloric effect, which makes them suitable for application as AMR materials for hydrogen liquefaction.

ACKNOWLEDGMENTS

The Ames Laboratory is operated for the U.S. Department of Energy by Iowa State University of Science and Technology under Contract No. DE-AC02-07CH11358. This work was supported by the Office of Basic Energy Sciences of the Office of Science of the U.S. DOE.

[1] J. H. Wernick and S. Geller, Trans. AIME **218**, 958 (1960).
[2] H. J. Williams, R. C. Sherwood, J. H. Wernick, and E. A. Nesbit, J. Phys. Soc. Jpn. (Suppl. B-1) **17**, 91 (1962).
[3] N. Nereson, C. Olsen, and G. Arnold, J. Appl. Phys. **37**, 4575 (1966).
[4] N. Nereson, C. Olsen, and G. Arnold, J. Appl. Phys. **39**, 4605 (1968).
[5] R. W. Hill and J. M. Machado da Silva, Phys. Lett. **30A**, 13 (1969).
[6] N. Kaplan, E. Dormann, K. H. J. Buschow, and D. Lebenbaum, Phys. Rev. B **7**, 40 (1973).
[7] H. J. Purwins and A. Leson, Adv. Phys. **39**, 309 (1990).
[8] W. M. Swift and W. E. Wallace, J. Phys. Chem. Solids **29**, 2053 (1968).
[9] K. A. Gschneidner, Jr., V. K. Pecharsky, and S. K. Malik, Adv. Cryog. Eng. **42**, 475 (1996).
[10] K. A. Gschneidner, Jr., H. Takeya, J. O. Moorman, and V. K. Pecharsky, Appl. Phys. Lett. **64**, 253 (1994).
[11] A. L. Lima, K. A. Gschneidner, Jr., V. K. Pecharsky, and A. O. Pecharsky, Phys. Rev. B **68**, 134409 (2003).
[12] R. Nirmala, Ya. Mudryk, V. K. Pecharsky, and K. A. Gschneidner, Jr., Phys. Rev. B **76**, 014407 (2007).
[13] K. A. Gschneidner, Jr., A. O. Pecharsky, and V. K. Pecharsky, in *Cryocoolers 11*, edited by R. S. Ross, Jr. (Kluwer Academic, Plenum, New York, 2001), p. 433.
[14] Y. L. Wu, A. O. Pecharsky, V. K. Pecharsky, and K. A. Gschneidner, Jr., Adv. Cryog. Eng. **48**, 3 (2002).
[15] K. A. Gschneidner, Jr., A. O. Pecharsky, Y. L. Wu, and V. K. Pecharsky, J. Solid State Chem. **171**, 324 (2003).
[16] K. W. H. Stevens, Proc. Phys. Soc. A **65**, 209 (1952).
[17] Materials Preparation Center, The Ames Laboratory U.S. Department of Energy, Ames, IA, USA, www.mpc.ameslab.gov
[18] V. K. Pecharsky, J. O. Moorman, and K. A. Gschneidner, Jr., Rev. Sci. Instrum. **68**, 4196 (1997).
[19] P. M. Levy and H. H. Chen, Phys. Rev. Lett. **27**, 1385 (1971).
[20] P. M. Levy, P. Morin, and D. Schmitt, Phys. Rev. Lett. **42**, 1417 (1979).
[21] M. Kosaka, H. Onodera, K. Ohoyama, M. Ohashi, Y. Yamaguchi, S. Nakamura, T. Goto, H. Kobayashi, and S. Ikeda, Phys. Rev. B **58**, 6339 (1998).
[22] M. Hiroi, M. Sera, N. Kobayashi, and S. Kunii, Phys. Rev. B **55**, 8339 (1997).
[23] K. A. Gschneidner, Jr. and V. K. Pecharsky, Annu. Rev. Mater. Sci. **30**, 387 (2000).
[24] V. K. Pecharsky and K. A. Gschneidner, Jr., J. Appl. Phys. **86**, 565 (1999).